Optimal Current Paths for Model Electrochemical Systems

Stanley J. Watowich and R. Stephen Berry*

Department of Chemistry and the James Franck Institute, The University of Chicago, Chicago, Illinois 60637
(Received: February 10, 1986)

Optimal control theory is used to determine process limits for a well-stirred fuel cell and a diffusive flow fuel cell, both operating with nonzero flows and in a finite time. Current paths and optimal end states are determined for cells constrained to provide either maximum work output, maximum effectiveness, or maximum profit. A constant current path is found to optimize these three criteria of process performance for the well-stirred fuel cell. In the diffusive flow fuel cell qualitatively different, nonmonotonic current trajectories are obtained for maximum work and maximum profit.

I. Introduction

In this paper we determine process limits, more realistic than reversible bounds, for electrochemical cells that operate at a nonzero rate and in a finite time. These cells deliver work and power through a fixed load and a variable resistance. The resistance can be adjusted to yield a time-parametrized current profile optimizing the different process variables of work output, effectiveness, and, as an economic measure, profit. Since the model systems include only current-dependent voltage losses and diffusive effects they serve as useful abstractions of realistic work-producing electrochemical cells, or fuel cells.

The performance of real systems frequently differs considerably from bounds based on equilibrium thermodynamics and reversible process paths.[1] Previous works have investigated the effect nonzero rate constraints and finite time operation have on performance bounds. More realistic performance limits have been found for Carnot-based heat engines,[2] for general endoreversible heat engines,[3] for internal combustion engines,[4] for distillation process,[5] and for intrinsically irreversible light-driven engines.[6] The last system cited has no reversible counterpart; the engine is necessarily driven by nonzero flows.

An effective tool to determine limits on the performance of processes occurring in a finite time is optimal control theory.[7] The value of this approach is that both the performance limit and the time path that yields this limit are obtained. All process variables associated with the operation of the system can be calculated once the time path is established.

The path optimization of the dynamic systems more appropriately falls under the heading of thermodynamics than do the parameter optimizations performed for processes in equilibrium or at steady state. These latter optimizations are best viewed as being within the domain of thermostatics. The state variables are constant and a performance criteria is maximized with respect to the system's parameters. The thermostatic approach is used by Bockris and Srinivasan[8] in their text of power and efficiency optimizations of fuel cells.

As mentioned, the limits found in this paper apply to processes occurring in a finite time. Rather than looking for the bound on a time-invariant electrochemical system, we ask what are realistic and meaningful bounds on work output, effectiveness, and profit and what process paths achieve these bounds when we set out to drain a closed well-stirred fuel cell within a fixed time. We also ask these questions for the case of a permeable, diffusive flow fuel cell, in which we also optimize its performance. In both these systems the initial state is fixed. The final state is free to be chosen to optimize the performance. This differs from a classical thermodynamic analysis for maximum work output in which the fuel cell would be drained from the initial state to the equipotential equilibrium state in an infinite time interval and along a reversible path.

The models used for the well-stirred fuel cells and the diffusive flow fuel cells are described in section II. Section III details the optimal control analysis as applied to the well-stirred cell. Analytic solutions are obtained for the performance criteria of maximum work output, maximum effectiveness, and maximum profit. Section IV contains the optimal control analysis of the diffusive flow cell. Solutions for the optimal current path are given by a set of coupled, nonlinear differential equations with mixed boundary conditions. These equations are solved numerically. In section V we discuss the effects both the rate-dependent and non-rate-dependent parameters have on the process limits.

II. Description of the Model

Consider the model electrochemical system shown in Figure 1. The reducing and oxidizing electrolytic solutions are separated into distinct compartments by a semipermeable membrane. Only nonreacting ions pass through the membrane, ensuring the electroneutrality of each compartment. The inert electrodes in contact with the two solutions are connected through an external circuit consisting of a load and a variable resistance. Power output is delivered at the load; this electrochemical system operates as a fuel cell.

Section II, A and B, describes the well-stirred fuel cell. In section IIC we add a diffusive term to these model systems to form the diffusive flow fuel cell. Overvoltage losses occurring at the electrodes are not included in the models outlined in section IIA and C. Including these losses, as done in section IIB, does not affect the general form of the current time path providing maximum work output, effectiveness, or profit for the well-stirred system.

The model fuel cell discussed in this paper operates with the following assumptions.

(i) Current density is spatially uniform.

(ii) The temperature of each system is spatially homogeneous and constant along the process path. This constraint assumes the entropy of reaction is zero,[8] no phase changes occur, mixing effects are negligible, the heat capacity of the system remains constant, and heating from electrical work and stirring is negligible. If the heat capacity or the volume of the system is large, the Ohmic loss heating does not produce a temperature change. No heat transfer need occur either across the membrane or across the walls of the cell. Alternatively, the above constraints can be relaxed and the

(1) Andersen, B.; Berry, R. S.; Ondrechen, M.; Salamon, P. *Acc. Chem. Res.* **1984**, *17*, 266.
(2) Curzon, F. L.; Ahlborn, B. *Am. J. Phys.* **1975**, *43*, 22. Salamon, P.; Nitzan, A. *J. Chem. Phys.* **1981**, *74*, 3546.
(3) Fairén, V.; Ross, J. *J. Chem. Phys.* **1981**, *75*, 5485, 5490. Rubin, M. H. *Phys. Rev. A* **1979**, *19*, 1272, 1277; **1980**, 1741. Salamon, P.; Band, Y. B.; Kafri, O. *J. Appl. Phys.* **1982**, *53*, 197.
(4) Hoffmann, K. H.; Watowich, S. J.; Berry, R. S. *J Appl. Phys.* **1985**, *58*, 2125. Mozurkewich, M.; Berry, R. S. *J. Appl. Phys.* **1982**, *53*, 34.
(5) Mullins, O.; Berry, R. S. *J. Phys. Chem.* **1984**, *88*, 723.
(6) Mozurkewich, M.; Berry, R. S. *J. Appl. Phys.* **1983**, *54*, 3651. Watowich, S. J.; Hoffmann, K. H.; Berry, R. S. *J. Appl. Phys.* **1985**, *58*, 2893.
(7) Bryson, A. E.; Ho, Y. C. *Applied Optimal Control*; Wiley: New York, 1975. Gottfried, B. S.; Weisman, J. *Introduction to Optimization Theory*; Prentice-Hall: Englewood Cliffs, NJ, 1973.
(8) Bockris, J.; Srinivasan, S. *Fuel Cells: Their Electrochemistry*; McGraw Hill: New York, 1969.

0022-3654/86/2090-4624$01.50/0

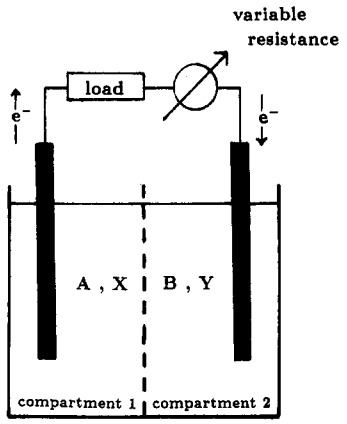

Figure 1. Model fuel cell.

cell could be placed in isothermal contact with a heat bath. The entropy production from heat flow between the bath and the cell compartments can then be incorporated into a minimization of entropy production.

(iii) No side reactions or electrode reactions (e.g., corrosion) occur. The anodic and cathodic reactions are respectively

$$\begin{aligned} A &\rightleftharpoons X + ne^- \\ B + ne^- &\rightleftharpoons Y \end{aligned} \qquad (I)$$

The initial concentrations of the reacting species are A_0, B_0, X_0, and Y_0.

(iv) The cell potential across the electrodes[8] (neglecting overpotential losses) is

$$E = E_r - IR_i \qquad (1)$$

where I is the current and E_r is the thermodynamic reversible potential of the cell given by

$$E_r = E^\circ - \frac{RT}{nF} \ln\left(\frac{N_X N_Y}{N_A N_B}\right) \qquad (2)$$

E° is the standard cell potential for the redox reaction $A + B \rightleftharpoons X + Y$. The IR_i term is the voltage drop due to Ohmic losses from the internal cell resistance R_i. The volume in each compartment of the cell is fixed at identical values.

These general considerations apply to each model electrochemical system discussed below. We now examine the specifics of each system, corresponding in turn to a well-stirred fuel cell, a well-stirred fuel cell with overpotential losses, and a diffusive flow fuel cell.

A. Well-Stirred Fuel Cell. We assume each compartment of the fuel cell is well stirred. The concentrations of the electrolyte species are spatially homogeneous and uniform. The time evolution of species A is

$$\frac{dN_A}{dt} = -\frac{I}{nF} \qquad (3)$$

where N_j is the moles of species j, n is the number of electrons transferred in reaction I, and F is Faraday's constant. Current flow favoring production of species X and Y is considered positive. Employing the dimensionless variables $\xi = (A_0 - A)/A_0$, $\nu = E/E^\circ$, $\tau = t/t_f$, and $\iota = It_f/(A_0nF)$ for the concentration, potential difference across the electrodes, time, and current, respectively, we rewrite eq 1–3 as

$$\nu = 1 - 2\beta_1 \ln\left(\frac{\beta_2 + \xi}{1 - \xi}\right) - \beta_4 \iota \qquad (4)$$

and

$$\dot{\xi} = \iota \qquad (5)$$

The dimensionless parameters are $\beta_1 = RT/(nFE^\circ)$, $\beta_2 = X_0/A_0$, and $\beta_4 = R_iA_0nF/(E^\circ t_f)$. We have assumed that $X_0 = Y_0$, $A_0 = B_0$, and $n = 1$. The dot notation is $d(\,)/d\tau$. The initial condition for eq 5 is $\xi = 0$ at $\tau = 0$.

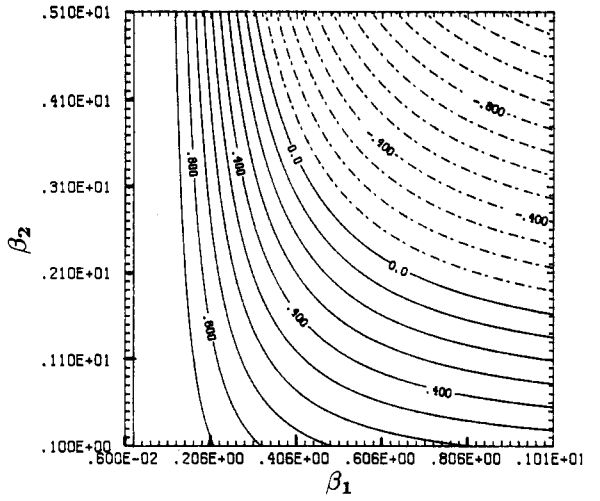

Figure 2. Contour plot of ξ_{eq} in (β_1, β_2) parameter space. Contour interval of 0.10.

The uppermost bound on work output for the well-stirred fuel cell is obtained by operating along a reversible path. Work output along this path is

$$\Gamma_{rev} = \int_0^{\xi(1)} 1 - 2\beta_1 \ln\left(\frac{\beta_2 + \xi}{1 - \xi}\right) d\xi = \xi(1) - 2\beta_1[(\beta_2 + \xi(1))\ln(\beta_2 + \xi(1)) - \beta_2 \ln(\beta_2) + (1 - \xi(1)) \ln(1 - \xi(1))] \qquad (6)$$

The end concentration $\xi(1)$ maximizing Γ_{rev} is the equilibrium concentration ξ_{eq}, given by

$$\xi_{eq} = \left(\exp\left(\frac{1}{2\beta_1}\right) - \beta_2\right) \Big/ \left(\exp\left(\frac{1}{2\beta_1}\right) + 1\right)$$

The equilibrium concentration, plotted in Figure 2 as contours in (β_1, β_2) parameter space, is a convenient base line against which to compare the end concentrations of optimized finite time processes. The dashed contours, representing negative values of ξ_{eq}, delineate regions in parameter space where the reverse of reaction I occurs. As β_1 increases, ξ_{eq} decreases; the driving force due to the standard cell potential decreases and the equilibrium shifts to the left in reaction I. Likewise, ξ_{eq} decreases as β_2 increases; the driving force due to the initial concentration gradient decreases and the equilibrium again shifts to the left.

B. Overpotential Losses. The difference in potential across the electrodes when current is flowing and when the circuit is open is the overpotential. With overpotential losses the voltage across the electrodes can be expressed as[8]

$$E = E_r - \eta_{act,c} - \eta_{conc,c} - \eta_{act,a} - \eta_{conc,a} - R_iI$$

The subscripts act and conc denote the contributions from activation overpotential and concentration overpotential, respectively. Activation overpotential is the extra potential needed to reduce the energy barrier of the rate-determining step of reaction I. Concentration overpotential is the loss resulting from limits on diffusion transfer of the reactants to, or products from, the electrode. The subscripts c and a reference reactions at the cathode and anode, respectively. In the linear Tafel region

$$\eta_{act,c} = \frac{RT}{\alpha_c F} \ln\left(\frac{I}{A_c I_{0,c}}\right)$$

and

$$\eta_{conc,c} = \frac{-RT}{nF} \ln\left(1 - \frac{I}{A_c I_{L,c}}\right)$$

A_c is the cathode surface area, α_c is the transfer coefficient for

the cathodic reaction, $I_{0,c}$ is the exchange current density (i.e., the velocity of the cathodic reaction at equilibrium), and $I_{L,c}$ is the limiting current density at the cathode. Similar expressions hold for the anodic reaction. In terms of the dimensionless variables introduced earlier

$$\nu = 1 - 2\beta_1 \ln\left(\frac{\beta_2 + \xi}{1 - \xi}\right) - \beta_c \ln(\gamma_c \iota) + 2\beta_1 \ln(1 - \gamma\iota) - \beta_a \ln(\gamma_a \iota) - \beta_4 \iota \quad (7)$$

where

$$\beta_c = RT/(\alpha_c FE^\circ) \qquad \beta_a = RT/(\alpha_a FE^\circ)$$
$$\gamma_c = A_0 nF/(t_f A I_{0,c}) \qquad \gamma_a = A_0 nF/(t_f A I_{0,a})$$

and

$$\gamma = A_0 nF/(t_f A I_L)$$

We have set $A_c = A_a = A$ and $I_{L,c} = I_{L,a} = I_L$.

In eq 7 the potential difference is a function of only the extent of reaction and current flow. It may be expressed as the sum of two univariable functions

$$\nu = \nu(\xi, \iota) = f(\xi) + g(\iota) \quad (8)$$

In section III we show that the functional form of the optimal current path for the well-stirred cell is the same for electrochemical systems with overpotential losses and without overpotential losses.

C. Diffusive Flow Fuel Cell. In this section we probe the effect of a nonzero diffusion rate on the behavior of the model electrochemical system. The potential difference across the electrodes is given by eq 4; overpotential losses are not included in this model. We assume the electrodes are immersed in infinite reservoir compartments. The concentration of species A in the bulk in compartment 1 of Figure 1 is A_0; if no current flow occurs in the cell then $A \rightarrow A_0$ at every point in compartment 1. Similarly for species X in compartment 1; $X_{bulk} = X_0$ and $X \rightarrow X_0$ at all points when no current flows. Assuming diffusion is proportional to the difference in concentration at the electrode surface and in the bulk, the time evolution of species A in compartment 1 can be written as

$$\dot{\xi} = \iota - \delta\xi \quad (9)$$

where δ is the dimensionless diffusion coefficient. This Fick's law approximation neglects contributions to concentration flux from convection and migration in the electric field. For simplicity, each reacting species in reaction I may be described by an expression similar to eq 9.

The well-stirred electrochemical cell has no steady-state position from which work, let alone power, can be extracted. However, the diffusion flow fuel cell bridges two infinite reservoirs of differing electrochemical potential. If unconstrained, the fuel cell would evolve to a steady state. The resulting current flow across the potential gradient would generate both work and power.

Assuming the external load and resistance across the electrodes can be set arbitrarily, it is useful to determine the maximum power obtainable from operating the cell at a steady state. This value provides a measure against which to compare the work output from optimized diffusive flow fuel cells. From eq 9 the steady-state current is

$$\iota_s = \delta\xi_s$$

Power output Φ at the steady state is

$$\Phi_s = \nu_s \iota_s$$

Maximizing Φ_s with respect to ξ_s gives

$$1 - 2\beta_4\delta\xi_s - \frac{2\beta_1(1 + \beta_2)\xi_s}{(\beta_2 + \xi_s)(1 - \xi_s)} = 2\beta_1 \ln\left(\frac{\beta_2 + \xi_s}{1 - \xi}\right)$$

where ξ_s is the optimal steady-state concentration at the electrode surface. In Figure 3a and b, contours of ξ_s and Φ_s, respectively, are plotted in (β_1, β_1) parameter space. Increasing either β_4 or

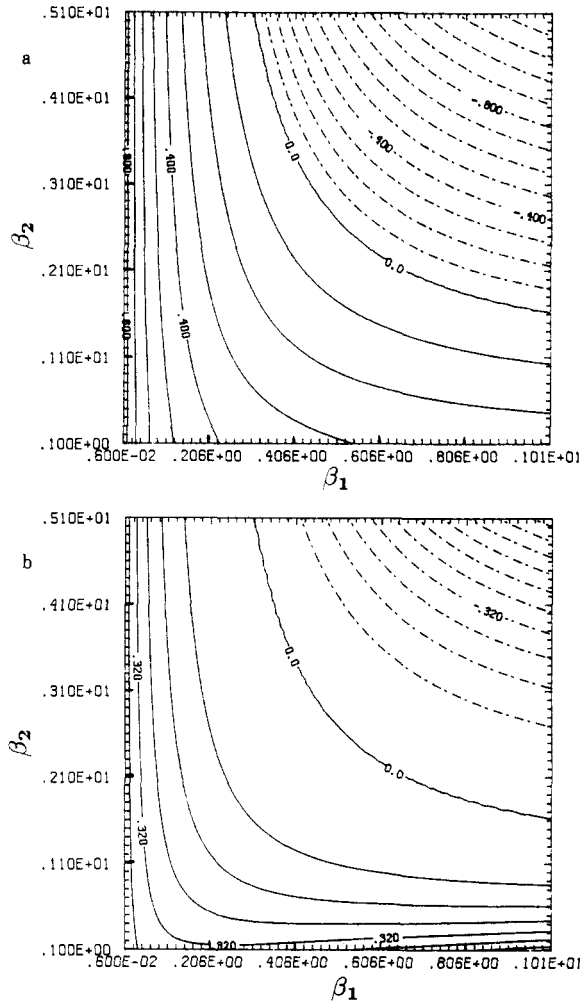

Figure 3. (a) Contour plot of ξ_s for the diffusive flow fuel cell in (β_1, β_2) parameter space. Contour interval of 0.10. $\beta_4 = 0.5$, $\delta = 1.0$. (b) Contour plot of Φ_s for the diffusive flow fuel cell in (β_1, β_2) parameter space. Contour interval of 8.0E-2. $\beta_4 = 0.5$, $\delta = 1.0$.

δ shifts the contours up and to the right, decreasing both ξ_s and Φ_s. However, the contour $\xi_s = 0$ in Figure 3a remains invariant, cutting the parameter space at $\beta_2 = \exp(1/(2\beta_1))$, regardless of the β_4 and δ values. The contours $\xi_{eq} = 0$, $\xi_s = 0$, and $\Phi_s = 0$ are identical.

III. Optimal Control of the Well-Stirred Cell

A. Maximum Work Output. In this section we determine both the current path and the end concentration that yield maximum work output from the well-stirred fuel cell operating in a finite time interval. The form of the current path is shown to be the same for all systems where the potential losses are functions of only the current. Thus, the current paths are the same for the two models of the well-stirred fuel cell looked at in this paper.

The objective function for maximum work output is

$$\Gamma = \int_{\tau_i}^{\tau_f} \nu\iota \, d\tau \quad (10)$$

The integration limits are $\tau_i = 0$ and $\tau_f = 1$. The scale for work output is $\Gamma = W/\beta_3$ where $\beta_3 = E^\circ A_0 nF$. With eq 5 as a differential constraint on the state variable ξ, the Hamiltonian for this system is written as

$$H = \nu\iota + \lambda\iota \quad (11)$$

The functional form of the control variable ι is

$$\frac{\partial H}{\partial \iota} = 0 = 1 - 2\beta_1 \ln\left(\frac{\beta_2 + \xi}{1 - \xi}\right) - 2\beta_4\iota + \lambda \quad (12)$$

The time evolution of the Lagrange multiplier λ is

$$\dot{\lambda} = \frac{-\partial H}{\partial \xi} = \frac{2\beta_1(1 + \beta_2)\iota}{(\beta_2 + \xi)(1 - \xi)} \tag{13}$$

Equations 5 and 13 can be solved simultaneously to give

$$\lambda = 2\beta_1 \ln\left(\frac{\beta_2 + \xi}{1 - \xi}\right) + c_0 \tag{14}$$

Substituting this expression into eq 12 gives

$$\iota = \frac{c_0 + 1}{2\beta_4} \tag{15}$$

Since ι is a function of constants, maximum work output occurs when the current is constant. Equation 5, describing the time evolution of the concentration, can be solved to give

$$\xi = \frac{(c_0 + 1)\tau}{2\beta_4} \tag{16}$$

From this expression we find $c_0 = 2\beta_4\xi(1) - 1$. Equation 10 can now be integrated along the optimal current path to give

$$\Gamma = \xi(1) - 2\beta_1[(\beta_2 + \xi(1)) \ln (\beta_2 + \xi(1)) + (1 - \xi(1)) \ln (1 - \xi(1)) - \beta_2 \ln (\beta_2)] - \beta_4\xi(1)^2 \tag{17}$$

as the upper bound on work output from a well-stirred fuel cell being drained from $\xi(0) = 0$ to $\xi(1)$ in a finite time interval.

Since the end concentration $\xi(1)$ is not constrained, a necessary boundary condition at τ_f is $\lambda(1) = 0$.[7] Given the boundary conditions, the optimal end concentration $\xi(1)$ is found by solving

$$1 - 2\beta_4\xi(1) = 2\beta_1 \ln\left(\frac{\beta_2 + \xi(1)}{1 - \xi(1)}\right) \tag{18}$$

Equation 18 can be solved numerically or $\xi(1)$ can be approximated by

$$\xi(1) \approx (1 - 2\beta_1 \ln (\beta_2))/\left(2\beta_1 + 2\beta_4 + \frac{2\beta_1}{\beta_2}\right)$$

Alternatively, the optimal end concentration can be related to the equilibrium concentration of the system as

$$\left(\frac{\beta_2 + \xi_{eq}}{1 - \xi_{eq}}\right)\Big/\left(\frac{\beta_2 + \xi(1)}{1 - \xi(1)}\right) = \exp\left(\frac{\beta_4\xi(1)}{\beta_1}\right)$$

In Figure 4 are plotted contours of optimal $\xi(1)$ in (β_1, β_2) parameter space. In Figure 5 are plotted contours of maximum work output, eq 17, in (β_1, β_2) space. The end values $\xi(1)$ in these curves were found by solving eq 18. In these figures the contour lines move down and to the left as β_4 increases. Higher Ohmic resistance R_i, or shorter operating interval t_f, shifts the optimal end concentration, and hence the work output, to smaller values. This reduces the current flowing through the cell and minimizes Ohmic losses. At low β_4 values the optimal $\xi(1)$ and Γ decrease as β_1 and β_2 increase, not unlike the behavior noted for the reversible cell. However, as β_4 increases, the (β_1, β_2) space separates into two regimes; at small β_2, $(\partial\Gamma/\partial\beta_1)_{\beta_2} > 0$, while at large β_2, $(\partial\Gamma/\partial\beta_1)_{\beta_2} < 0$. The region where $(\partial\Gamma/\partial\beta_1)_{\beta_2} > 0$ is termed the favored work region. The unfavored work region occurs where $(\partial\Gamma/\partial\beta_1)_{\beta_2} < 0$.

Additional current-dependent losses (e.g., overpotential losses), if included in the expression for the potential difference across the electrode, do not change the form of the current path generating optimal work output. The potential difference in this case is given by eq 8. The Hamiltonian is given by eq 11. The control variable ι is implicitly determined by

$$\frac{\partial H}{\partial \iota} = 0 = f(\xi) + g(\iota) + \iota\frac{dg(\iota)}{d\iota} + \lambda \tag{19}$$

The Lagrange multiplier evolves as

$$\dot{\lambda} = -\iota\frac{df(\xi)}{d\xi} \tag{20}$$

Solving eq 5 and 20 simultaneously yields

$$\lambda = -f(\xi) + c_1 \tag{21}$$

and

$$g(\iota) + \iota\frac{dg(\iota)}{d\iota} + c_1 = 0 \tag{22}$$

With the boundary condition $\lambda(1) = 0$ this equation simplifies to

$$g(\iota) + \iota\frac{dg(\iota)}{d\iota} + f(\xi(1)) = 0$$

The current is constant along the path that maximizes work output and depends upon the final concentration.

B. Maximum Effectiveness. Effectiveness, or the second-law efficiency, can be expressed as

$$\epsilon = \Gamma/\Gamma_{rev}$$

where W_{rev} is given by eq 6 and is a function of $\xi(1)$ alone. Both the reversible process and the process occurring in finite time operate between the same initial and final states. The maximum possible work output for the well-stirred fuel cell is given by eq 17. We can rewrite the effectiveness as

$$\epsilon = 1 - \frac{\beta_4\xi(1)^2}{\Gamma_{rev}}$$

The maximum path problem simplifies to an optimization of ϵ with respect to $\xi(1)$. The effectiveness is optimized along the boundary maximum $\iota = 0$ and $\xi(1) = 0$, at which point $\epsilon = 1$. For the parameter sets studied, no interior, local maximum is found.

In Figure 6 are overlaid contours of effectiveness on maximum work output contours in (β_1, β_2) space. The end concentrations maximize work output. The contours of effectiveness move up and to the left as β_4 decreases; smaller Ohmic losses are possible at lower values of β_4. Of particular interest is the magnitude of the effectiveness; the effectiveness remains in the range 0.49–0.65 for $0.5 \leq \beta_4 \leq 10.0$. In the unfavored work region effectiveness increases as work decreases. In the favored work region both the effectiveness and work output increase as β_1 increases.

C. Maximum Profit. Following Salamon and Nitzan[2] we view the fuel cell as a production process with work as an output and species A and B as inputs. Given an initial input of the reacting species, the problem we face is to operate the fuel cell within a finite time period while maximizing a profit function. The profit function[9] is the difference between revenue and costs, which for a simple system with perfect competition is

$$P = R - C = p_o\Gamma_{Net} - p_i(A_0 - A) \tag{23}$$

The prices per unit of input and output, p_i and p_o, respectively, are constant in an economic model assuming perfect competition. Costs incurred in the process are assumed to depend only on the quantity of inputs consumed. This model neglects long-term costs associated with maintainance, depreciation, and capital investment. The short-run optimization performed below treats the system parameters as constants in the time period considered.

In the dimensionless variables, eq 23 can be scaled to give

$$\Pi = \int_0^1 (\beta_5\nu\iota - \iota)\, d\tau \tag{24}$$

where $\Pi = P/A_0p_i$, $\beta_5 = p_oE^\circ nF/p_i$, and ν is given by eq 4. The Hamiltonian for this objective function is

$$H = (\nu - 1/\beta_5)\beta_5\iota + \lambda\iota$$

In this form it is easily seen that profit maximization can be treated as a special case of overvoltage loss; the potential difference is

(9) Kohler, H. *Intermediate Microeconomics: Theory and Applications*; Scott, Foreman: Glenview, IL, 1982.

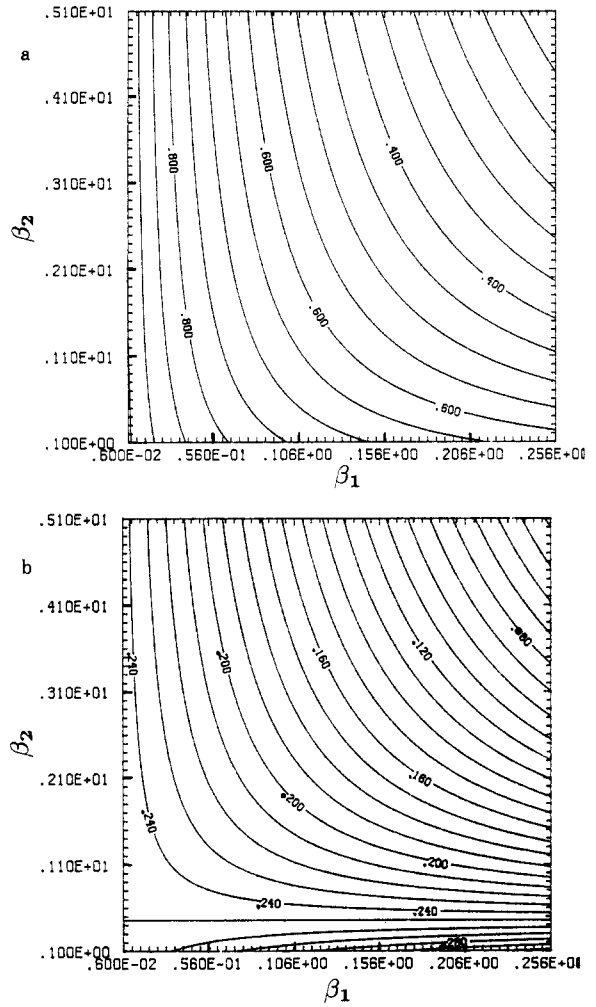

Figure 4. (a) Contour plot of optimal $\xi(1)$ for maximum work output from the well-stirred fuel cell in (β_1, β_2) parameter space. Contour interval of 5.0E-2. $\beta_4 = 0.5$. (b) Contour plot of optimal $\xi(1)$ for maximum work output from the well-stirred fuel cell in (β_1, β_2) parameter space. Contour interval of 1.0E-2. $\beta_4 = 2.0$.

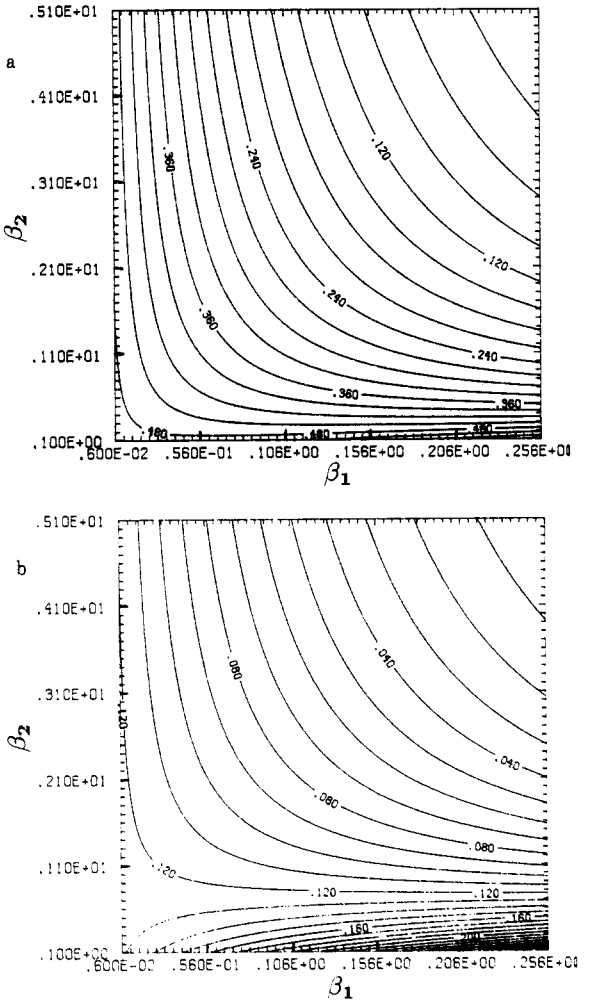

Figure 5. (a) Contour plot of Γ for maximum work output from the well-stirred fuel cell in (β_1, β_2) parameter space. Contour interval of 3.0E-2. $\beta_4 = 0.5$. (b) Contour plot of Γ for maximum work output from the well-stirred fuel cell in (β_1, β_2) parameter space. Contour interval of 1.0E-2. $\beta_4 = 2.0$.

diminished by a constant loss term rather than a current-dependent loss term. The optimal current path is constant and the optimal extent of the reaction is found by solving

$$2\beta_1 \ln\left(\frac{\beta_2 + \xi(1)}{1 - \xi(1)}\right) = 1 - \frac{1}{\beta_5} - 2\beta_4\xi(1) \qquad (25)$$

for $\xi(1)$. When $p_o \gg p_i$ the optimal profit solution approaches the optimal work output solution. At the other extreme, when $\xi(1) \leq 0$ it is no longer profitable to run the fuel cell, even along the optimal process path. This unprofitable condition occurs for $\beta_5 \leq 1/(1 - (2\beta_1 \ln \beta_2))$.

The explicit evaluation of eq 24 is similar to the determination of maximum work output. The optimal profit is found as a function of $\xi(1)$. In Figure 7 are plotted contours of optimal $\xi(1)$ for profit maximization in (β_1, β_2) space. The optimal $\xi(1)$ contour moves up and to the right as β_5 increases and β_4 decreases. As the price per unit output relative to the price per unit input increases the profit optimum requires more inputs be consumed and more outputs produced. Again a bifurcation in (β_1, β_2) parameter space is observed for the β_2 parameter.

IV. Diffusive Flow Fuel Cell

A. Maximum Work Output. With the objective function given by eq 10 and the differential constraint given by eq 9, the Hamiltonian for diffusive flow fuel cell is

$$H = \nu\iota + \lambda(\iota - \delta\xi) \qquad (26)$$

Since the major loss mechanism studied in this model is Ohmic loss, the potential difference across the electrodes is described by eq 4. The time evolution of the adjoint variable λ is

$$\dot{\lambda} = \frac{2\beta_1(1 + \beta_2)\iota}{(\beta_2 + \xi)(1 - \xi)} + \delta\lambda \qquad (27)$$

Maximizing the Hamiltonian by setting $\partial H/\partial\iota = 0$ gives

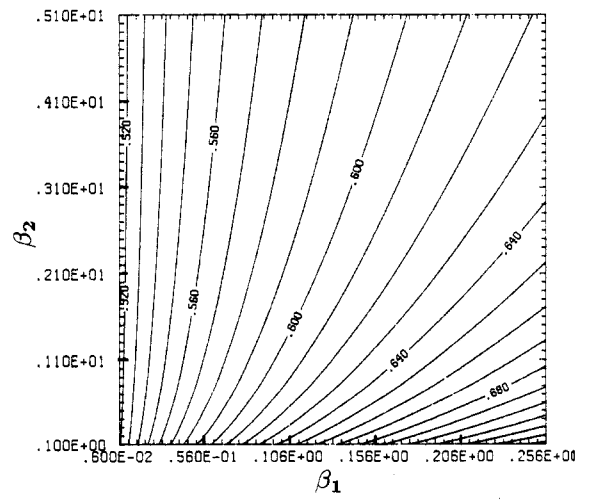

Figure 6. Contour plots of Γ for maximum work output from the well-stirred fuel cell in (β_1, β_2) parameter space. Contour interval of 3.0E-2. $\beta_4 = 0.5$.

$$\iota = \frac{1}{2\beta_4}\left[1 - 2\beta_1 \ln\left(\frac{\beta_2 + \xi}{1 - \xi}\right) + \lambda\right] \tag{28}$$

Substituting the above equation into eq 9 and 27 yields two coupled nonlinear differential equations. The boundary conditions on these equations are $\xi(0) = 0$ and $\lambda(1) = 0$. This system of equations is solved numerically by using a two-point boundary value solver.[6] The resulting path provides the maximum work output for a diffusive flow fuel cell.

For a representative (β_1, β_2, β_4, δ) parameter set, we plot both the optimal current path and the resulting concentration path in Figure 8. Unlike the well-stirred fuel cell, the optimal current path for the diffusive flow cell is not a constant. As β_1 increases, the dip in the current path becomes more pronounced. Figure 9 plots the potential difference against the current along the optimal work path. Figure 10 plots optimal $\xi(1)$ against δ for the diffusive flow cells, one cell maximizing work output and the other cell maximizing profit (see section IVB).

One measure of the effectiveness of the diffusive flow cell along the optimal work path is

$$\epsilon = \Gamma/\Gamma_D$$

where

$$\Gamma_D = \int_{\tau_i}^{\tau_f}\left(1 - 2\beta_1 \ln\left(\frac{\beta_2 + \xi}{1 - \xi}\right)\right)\iota \, d\tau$$

would be the work output if Ohmic losses were not present. In this paper we do not look for local internal optima for the effectiveness of the diffusive flow fuel cell. The global maximum occurs at the boundary value $\iota = 0$ and $\xi(1) = 0$. Figure 11 plots work output Γ and effectiveness ϵ against the diffusive coefficient δ for the diffusive cell maximizing work output. Increasing δ decreases the effectiveness and increases the work output. Increasing β_4 decreases both the effectiveness and the work output.

B. Maximum Profit. For the diffusive flow fuel cell the Hamiltonian maximizing the profit functional, given by eq 24, is

$$H = (\nu - (1/\beta_5))\beta_5 \iota + \lambda(\iota - \delta\xi) \tag{29}$$

The optimal current path is

$$\iota = \frac{1}{2\beta_4\beta_5}\left(-2\beta_1 \ln\left(\frac{\beta_2 + \xi}{1 - \xi}\right) + \lambda\right)$$

The time evolution of ξ and λ along the optimal current path is necessarily given by eq 9 and

$$\dot{\lambda} = \frac{2\beta_1(1 + \beta_2)\beta_5\iota}{(\beta_2 + \xi)(1 - \xi)} + \delta\xi$$

respectively. As before, the boundary conditions are $\xi(0) = 0$ and $\lambda(1) = 0$. The coupled, nonlinear differential equations are solved numerically to give the explicit optimal current path.

In Figure 12 are plotted the optimal current and concentration paths for several β_5 parameter sets. As β_5 is increased, the end concentration, current level, and work output drop. The optimal current path shifts dramatically from a left skewed parabola for $\beta_5 = 0.5$, to a roughly symetric parabola for $\beta_5 = 1.0$, to a right skewed parabola for $\beta_5 = 2.0$.

V. Discussion and Summary

Work output, effectiveness, and profit are maximized in the well-stirred fuel cell when the current through an external load is held constant during the finite time interval of operation. This path occurs for all current-dependent losses. In cells maximizing work output and profit such a path minimizes the overpotential losses while sustaining the highest possible power production. Maximum effectiveness occurs for the boundary optimum $\iota = 0$. The constant current operation is similar to optimal process paths reported by Mozurkewich and Berry[4] and by Salamon et al.[10] In the first case a constant velocity piston path maximized work output along the nonpower strokes of an Otto engine. In the second case a constant-temperature path minimized entropy production in a endoreversible heat engine.

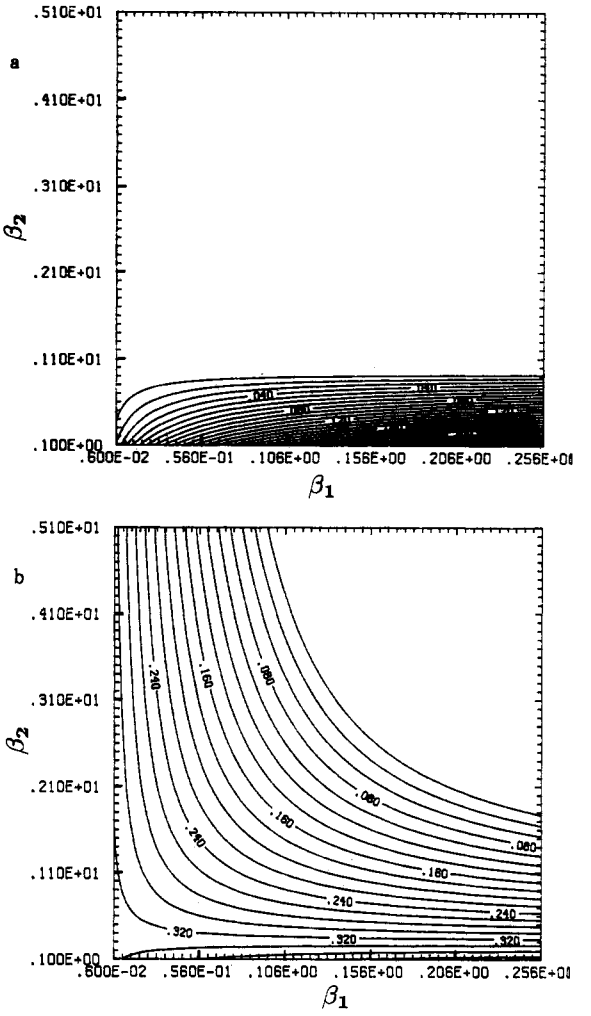

Figure 7. (a) Contour plot of optimal $\xi(1)$ for profit maximization of the well-stirred fuel cell in (β_1, β_2) parameter space. Contour interval of 1.0E-2. $\beta_4 = 0.5$. $\beta_5 = 1.0$. (b) Contour plot of optimal $\xi(1)$ for profit maximization of the well-stirred fuel cell in (β_1, β_2) parameter space. Contour interval of 2.0E-2. $\beta_4 = 0.5$. $\beta_5 = 1.5$.

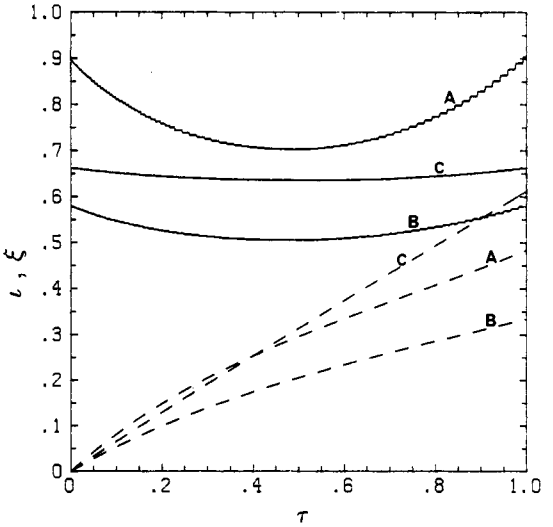

Figure 8. Current (solid curve) and concentration (dashed curve) profiles for maximum work output from the diffusive flow fuel cell. $\beta_1 = 0.25$. $\beta_2 = 0.15$. Curve assignments: $\beta_4 = 0.5$ and $\delta = 1.0$ (A); $\beta_4 = 1.0$ and $\delta = 1.0$ (B); $\beta_4 = 0.5$ and $\delta = 0.1$ (C).

(10) Salamon, P.; Nitzan, A.; Andersen, B.; Berry, R. S. *Phys. Rev. A* **1980**, *21*, 2115.

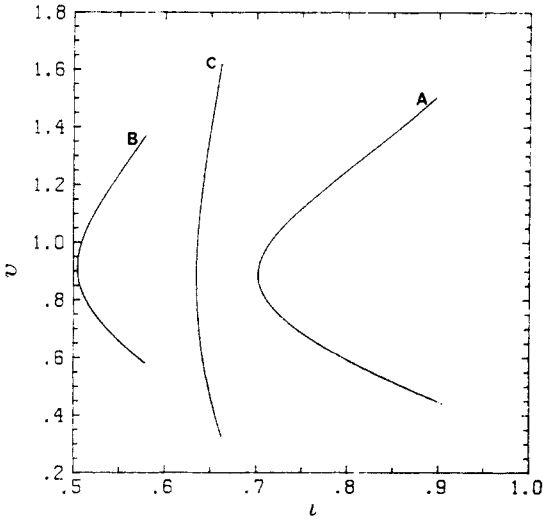

Figure 9. Time-parametrized curves of potential difference vs. current for maximum work output from the diffusive flow fuel cell. $\beta_1 = 0.25$. $\beta_2 = 0.15$. Curve assignments: $\beta_4 = 0.5$ and $\delta = 1.0$ (A); $\beta_4 = 1.0$ and $\delta = 1.0$ (B); $\beta_4 = 0.5$ and $\delta = 0.1$ (C).

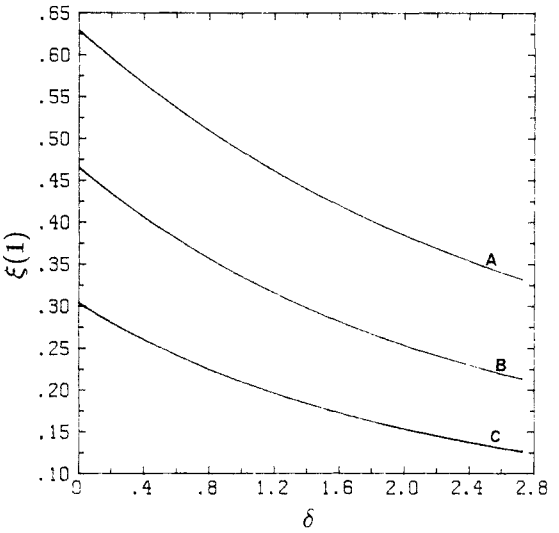

Figure 10. Optimal $\xi(1)$ plotted against δ for maximum work output from the diffusive flow fuel cell. $\beta_1 = 0.25$. $\beta_2 = 0.15$. Curve assignments: $\beta_4 = 0.5$ (A), $\beta_4 = 1.0$ (B), and $\beta_4 = 2.0$ (C).

The magnitude of the constant current path differs for the three performance criteria. The optimal $\xi(1)$ for maximum work output and effectiveness serve as natural bounds on the optimal $\xi(1)$ for maximum profit. Contour curves in (β_1, β_2) parameter space for $\xi(1)$ optimizing work output and profit approach the curves of ξ_{eq} when β_4 is low and β_5 is high. Optimal $\xi(1)$ for work and profit maximization is less than ξ_{eq}, implying that the well-stirred fuel cell is not completely drained.

The gradient of $\xi(1)$ in (β_1, β_2) space is much steeper for maximum work output than the gradient of ξ_{eq} in the same space. For low β_4 values both contours decrease as β_1 and β_2 increase; as the driving force from either the standard cell potential or the concentration potential decreases, $\xi(1)$ and Γ decrease. However, at large β_4 values a bifurcation occurs in the contours of optimal $\xi(1)$ and Γ for maximum work output and maximum profit. For constant β_2, a low β_2 region exists where both optimal $\xi(1)$ and Γ increase as β_1 increases. Thus a region, the work-favored region, exists in parameter space where increased work output and profit can be obtained from the well-stirred fuel cell by reducing the standard cell potential of the reacting electrolytic species. This effect is more pronounced at higher β_1 values.

The effectiveness of the well-stirred cells maximizing work output increases as β_1 increases and β_2 decreases. The Γ and ϵ curves in Figures 5 and 6 can guide future, more detailed studies aimed at improving fuel cells. Research should concentrate on

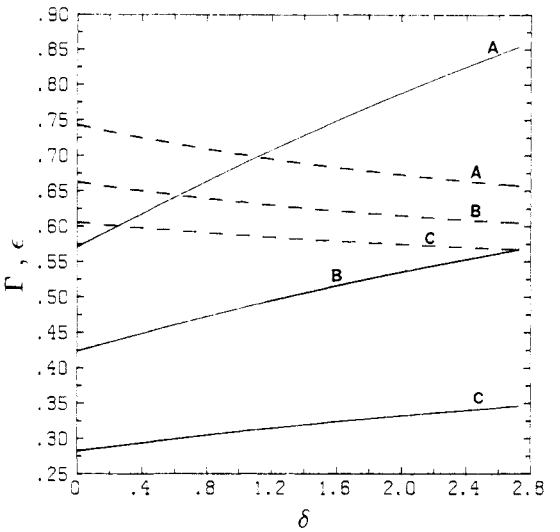

Figure 11. Work output Γ (solid curve) and effectiveness ϵ (dashed curve) plotted against δ for the diffusive flow fuel cell maximizing work output. $\beta_1 = 0.25$. $\beta_2 = 0.15$. Curve assignments: $\beta_4 = 0.5$ (A), $\beta_4 = 1.0$ (B), and $\beta_4 = 2.0$ (C).

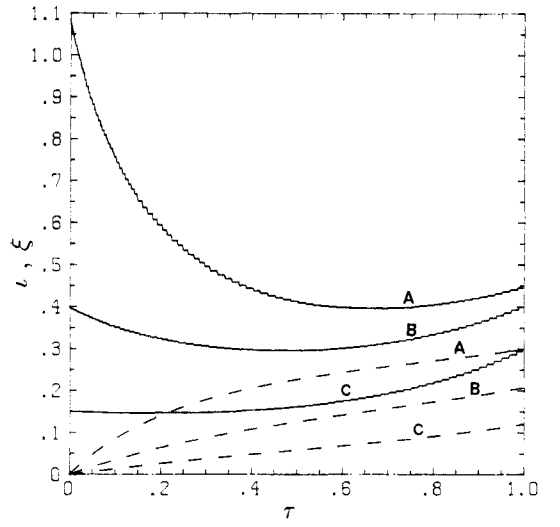

Figure 12. Current (solid curve) and concentration (dashed curve) profiles for profit maximization of the diffusive flow fuel cell. $\beta_1 = 0.25$. $\beta_2 = 0.15$. $\beta_4 = 0.5$. $\delta = 1.0$. Curve assignments: $\beta_5 = 0.5$ (A), $\beta_5 = 1.0$ (B), and $\beta_5 = 2.0$ (C).

the β_2 parameter since this analysis implies that it is possible to increase both the optimal work output and the effectiveness of the cell by decreasing β_2. A similar situation occurs for the β_1 only in the work-favored region; elsewhere changes in β_1 involve a tradeoff between increased optimal work output and decreased effectiveness.

At low β_5 values the profit-optimized well-stirred fuel cell displays a bifurcation similar to that between the work-unfavored and the work-favored region. Asymptotically increasing $\xi(1)$ and profit Π result for increases in β_1. This occurs most strongly at low β_4 and low β_5, where the price per unit input dominates the price per unit output. In this region we can decrease both the standard cell potential and the concentration potential (increase β_1 and β_2) and remain at the same profit level.

Analytic solutions for maximum work output and maximum profit are not found for the diffusive flow fuel cell. The optimal current paths are not constant over the finite time interval that the cell operates in. Instead, the current approaches a constant value as β_1, β_2, or δ decrease and β_4 increases. The general form of the current path maximizing work output is an upward opening parabola, with a minimum occurring approximately midway along the time interval. As found for the well-stirred fuel cell, work output decreases as β_4 increases. As δ increases the optimal work

output decreases and the effectiveness increases.

The optimized diffusive flow fuel cell can deliver twice the work as the steady-state diffusive flow cell. This result suggests novel designs for fuel cells constructed to provide maximum work output. For example, if the reactants are inexpensive, one can run a cell along an optimal work path followed by a recharge of the cell at the end of the cycle interval. Such a cyclic operation would deliver more work and average power than a diffusive cell in a steady-state operation.

It should be possible to construct both the well-stirred fuel cell and the diffusive flow fuel cell. A variable resistance can be programmed to constrain the current to the optimal path. Work output from fuel cells following the work-optimized current paths can be compared to the predicted optimal work output. This would provide a measure of how realistic and applicable the upper work bounds provided by the modeled fuel cells are to real processes. Additionally, the work-favored region predicted for the well-stirred fuel cell can be probed to determine if it exists in real electrochemical systems.

This paper extends the application of thermodynamics to simple electrochemical systems that can serve as generic models for fuel cells operating in a finite time and with nonzero flows. Several interesting behaviors are revealed in this analysis, not the least of which is the parabolic current path for maximum work output from the dissipative flow fuel cell. This work provides useful directions for the future study of performance limits of realistic models of fuel cells and photoelectrochemical cells. In more detailed models heat flows, side reactions, finite reaction rates, and electrode surface effects can be introduced. The inclusion of heat flows would allow the investigation of bounds on minimum entropy production.

Acknowledgment. This work was supported by Contract No. 5083-260-0834 with the Gas Research Institute, Chicago, Illinois.

CHEMICAL KINETICS

Subharmonic Response of a Heterogeneous Catalytic Oscillator, the "Cantabrator", to a Periodic Input

S. C. Capsaskis and C. N. Kenney*

Department of Chemical Engineering, University of Cambridge, Cambridge, U.K. *(Received: October 9, 1985; In Final Form: March 20, 1986)*

The oscillatory reaction between oxygen and carbon monoxide/propene mixtures, the Cantabrator, has been studied with periodic feed switching in order to investigate the interactions of complex reaction dynamics with a time-varying concentration input. A supported platinum catalyst was used in a continuously stirred tank reactor (CSTR) at 1 bar total pressure at temperatures in the range 408-423 K. Two instances of subharmonic response (in which the output oscillation has twice the input period), rarely discussed in heterogeneous catalytic oscillators, are reported. Our elementary step model, previously proposed to account for the spontaneous concentration oscillations of this and other CO/alkene systems under steady-feed conditions, is used to obtain qualitative and some quantitative insights into the occurrence of subharmonic response.

Introduction

The study of periodic feed switching in catalytic reactors is a specific example of the wider topic of "forcing" a system, mechanical, chemical, electrical or environmental, which may have a natural frequency of its own. Work to date has been mainly concerned with devising optimum switching schemes that could enhance reactor performance, as measured in terms of time-averaged conversion or reaction selectivity.

A plethora of reactions have been examined under conditions where the reactor feed concentration varies with time. These include the oxidation of sulfur dioxide on V_2O_5,[1] the oxidation of ethene on Ag,[2] the hydrogenation of butadiene on Ni,[3] the synthesis of ammonia,[4,5] the addition of ethene to acetic acid catalyzed by H_2SO_4,[6] the Fischer-Tropsch synthesis reaction,[7] and, last but not least, the oxidation of carbon monoxide. Hawkins[8] and Cutlip[9] reported significantly increased reaction rates of CO oxidation compared to the steady-state rate when two streams consisting of CO/argon and O_2/argon mixtures are alternatively fed to the reactor. The oxidation of CO on V_2O_5 has also been examined[10] as well as the oxidation of CO/NO mixtures.[12]

The work reported here is concerned with the more fundamental problem of the interaction of a time-varying reactor feed with the complex kinetics of the heterogeneous catalytic oxidation of a

(1) Unni, M. P.; Hudgins, R. R.; Silveston, P. L. *Can. J. Chem. Eng.* **1973**, *51*, 623-628.
(2) Renken, A.; Muller, M.; Wandrey, C. *Chem. React. Eng., Proc. Int. Symp., 4th* **1976**, 107-116; ISCRE-4
(3) Al-Taie, A. S.; Kershenbaum, L. S. *ACS Symp. Ser.* **1978**, *68*, 512-525.
(4) Jain, A. K.; Silveston, P. L.; Hudgins, R. R. *ACS Symp. Ser.* **1982**, *196*, 97-108.
(5) Jain, A. K.; Hudgins, R. R.; Silveston, P. L. *Can. J. Chem. Eng.* **1984**, *61*, 824-832.
(6) Renken, A.; Truffer, M.-A.; Dettmer, M. *IChemE Symp. Ser.* **1984**, 87.
(7) Feimer, J. L.; Silveston, P. L.; Hudgins, R. R. *Can. J. Chem. Eng.* **1984**, *62*, 241-248.
(8) Hawkins, C. J. Ph.D. Thesis, University of Cambridge, Cambridge, U.K., 1978.
(9) Cutlip, M. B. *AIChE. J.* **1979**, *25*, 502-508.
(10) Abdul-Kareem, H. K.; Jain, A. K.; Silveston, P. L.; Hudgins, R. R. *Chem. Eng. Sci.* **1980**, *35*, 273-277, 2077-2084.
(11) Rehmus, P.; Ross, J. In *Oscillations and Travelling Waves in Chemical Systems*; Field, R. J., Burger, M., Ed.; Wiley Interscience: New York, 1985.
(12) Hegedus, L. L.; Chang, C. C.; McEwen, D. J.; Sloane, M. *Ind. Eng. Chem. Fundam.* **1980**, *19*, 367-373.

0022-3654/86/2090-4631$01.50/0